The Use of Dispersion Relations in the $\pi\pi$ and $K\bar{K}$ Coupled Channel System

Zhiguang Xiao and Hanqing Zheng [*]

Department of Physics, Peking University, Beijing 100871,

People's Republic of China

Abstract

Systematic and careful studies are made on the properties of the IJ=00 $\pi\pi$ and $K\bar{K}$ coupled–channel system, using newly derived dispersion relations between the phase shifts and poles and cuts. The effects of nearby branch point singularities to the determination of the $f_0(980)$ resonance are estimated and discussed.

PACS numbers: 11.55 -m; 11.55Bq; 11.55Fv

---

[*]e-mail: zheng@th.phy.pku.edu.cn

1

I. INTRODUCTION

The physics related to the IJ=00 $\pi\pi$ and $K\bar{K}$ coupled–channel system, especially the property of the narrow $f_0(980)$ resonance, has been a subject of long and wide interests both experimentally and theoretically (For an incomplete list of references, see for example, Ref. [1] – [26]). In the latest version of Review of Particle Physics [27], the width of the $f_0(980)$ resonance is estimated to be about 40 to 100 MeV and it is remarked that the "width determination very model dependent". Previous estimates on the width of the $f_0(980)$ resonance may essentially be categorized into two classes: the first is the S matrix or T matrix pole fit, and the second is from the invariant mass fit in production experiments. It should be stressed that in a production experiment the spectrum is highly sensitive to the structure of the production vertex and therefore the invariant mass fit should not be considered as very accurate. A numerical calculation to the formfactor-like quantity in the coupled–channel system reveals [28] that the behavior of the coupled–channel form-factor around the $f_0(980)$ region is very fragile: it can easily generate a peak or a dip, and the difference only comes from the (bare) production vertices. For the S matrix fit or the T matrix fit, in the literature various models have been proposed to determine the pole position of the $f_0(980)$ narrow resonance. Different from these approaches we in this paper will use the dispersion techniques to study the IJ=00 $\pi\pi$ and $K\bar{K}$ coupled–channel system. The theory of dispersion relation starts directly from fundamental principles like unitarity and analyticity and when combining with experimental information the dispersion theory is predictive. As we will see from the discussion in this paper, the analytic structure around the $f_0(980)$ or the $K\bar{K}$ threshold region is very complicated: there are branch point singularities which are very close to the $f_0(980)$ pole, and it is out of question that one has to carefully examine the influence of these nearby branch point singularities to the determination of the pole location of the $f_0(980)$ resonance. Furthermore, the $\pi\pi$ scattering phase shift δ_π, as an analytic function defined in the single channel unitarity region, is different from the δ_π defined in the coupled–channel unitarity region and the two quantities have to be treated separately in using dispersion relations. Though the analytic structure around the $f_0(980)$ region is very complicated, physics related to the $f_0(980)$ resonance can be discussed by using properly established dispersion relations.

For the simpler case of $\pi\pi$ scatterings in the single channel approximation, we have in Ref. [29] set up a dispersion relation for the real part (defined in the physical region) of the T matrix which is related to the experimental observable $\sin(2\delta_\pi)$ by the following equation,

$$\sin(2\delta_\pi) = \rho \left(\sum_i \frac{i}{2\rho(z_i)S'(z_i)(z - z_i)} + \frac{1}{\pi} \int_L \frac{\text{Im}_L F}{s' - z} ds' \right) , \qquad (1)$$

in which $F \equiv T(1 + S)/S$ and F is equal to $2\text{Re}T$ in the physical region. In Eq. (1) the position of zeros of S on the physical sheet of the complex s plane are denoted as z_i. The discontinuity of F on the left–hand cut (l.h.c.), $L = (-\infty, 0]$ manifests itself in the left–hand integral on the r.h.s. of the above equation, where one subtraction to the integral is understood. A very attractive feature of Eq. (1) is that it explicitly shows the contributions from different types of dynamical singularities: the resonances and the left–hand cut (and bound states or virtual states can be easily included when necessary). Eq. (1) has proved to be useful in determining the pole position of the σ resonance [29], especially in clarifying

the role of the left–hand cut in the determination of the σ resonance. That is, the *l.h.c.* contribution to $\sin(2\delta_\pi)$ is negative and concave and therefore there must exist a σ resonance to explain the experimental data.

The aim of this paper, as stated above, is to extend the discussion of Ref. [29] to the more realistic case of the $IJ = 00$ $\pi\pi$ and $K\bar{K}$ coupled–channel system. We will set up dispersion representations for physical observables in which the unitarity cut contributions are dissolved and the dependence of a physical quantity on the left–hand cut (*l.h.c*) becomes explicit. The method proposed in this paper is rather general and can in principle be extended to more complicated situation with more than two channels as well.

The material of this paper is organized as follows: The Sec. II contains the theoretical discussions on the coupled–channel system. In Sec. II A the general property of the analytic structure of the $\pi\pi$ and $K\bar{K}$ coupled–channel system is reviewed, including the analytic continuation and the left–hand cuts. In Sec. II B, dispersion relations are set up for analytic functions constructed from the scattering T matrix. Such analytic functions contain no unitarity cut. In Sec. II C, the analytic properties of the newly constructed functions are analyzed in perturbation theory and in a simple narrow resonance model. The Sec. III is devoted to physical discussions using the dispersion relations founded in Sec. II. In Sec. III A the physical interpretation of the dispersion relation, Eq. (18), above the $K\bar{K}$ threshold is discussed. It is shown that the $\pi\pi$ scattering phase δ_π, defined above the $K\bar{K}$ threshold contains a branch point singularity at $s = 4m_K^2 - 4m_\pi^2$. In Sec. III B the dispersion relation for $\sin(2\delta_\pi)$ in the single channel unitarity region is established which is a generalization of Eq. (1) in the coupled–channel situation. The Sec. IV is for the application of our method in phenomenology where the property of the $f_0(980)$ resonance and the influence of the nearby branch point singularities to the determination of the pole location of $f_0(980)$ is carefully examined. In Sec.IV A a general discussion is given to $f_0(980)$ and its nearby branch point singularities and Sec. IV B is devoted to fitting the pole position of the $f_0(980)$ resonance combining the single channel and the coupled–channel dispersion relations set up in this paper. In Sec. IV C a subtlety in our procedure is discussed. The Sec. V is for the final conclusion.

II. THE ANALYTIC STRUCTURE OF $\pi\pi$ AND $K\bar{K}$ COUPLED–CHANNEL SYSTEM: GENERAL DISCUSSIONS

A. The analytic continuation on the Riemann surface

As is well known, the coupled–channel partial–wave scattering matrix, S, is discontinuous on the unitarity cut. In the two channel approximation the unitarity cut includes two kinematical singularities: the first one starts from $4m_\pi^2$ to ∞ whereas the second cut starts from $4m_K^2$ to ∞, which defines a four–sheets Riemann surface. The relation between the S matrix and the T matrix is,

$$
\begin{aligned}
S_{11} &= 1 + 2i\rho_1 T_{11}^I \ , \\
S_{22} &= 1 + 2i\rho_2 T_{22}^I \ , \\
S_{12} &= 2i\sqrt{\rho_1\rho_2}T_{12}^I \ .
\end{aligned}
$$

(2)

For the T matrix the unitarity relation on the unitarity cut reads,

$$\text{Im}T_{11} = T_{11}\rho_1 T_{11}^* \times \theta(s - 4m_\pi^2) + T_{12}\rho_2 T_{12}^* \times \theta(s - 4m_K^2) \,,$$
$$\text{Im}T_{12} = T_{12}\rho_2 T_{22}^* \times \theta(s - 4m_K^2) + T_{11}\rho_1 T_{12}^* \times \theta(s - 4m_\pi^2) \,,$$
$$\text{Im}T_{22} = T_{22}\rho_2 T_{22}^* \times \theta(s - 4m_K^2) + T_{12}\rho_1 T_{12}^* \times \theta(s - 4m_\pi^2) \,, \tag{3}$$

where $T_{12} = T_{21}$ has been used. The kinematic factors ρ_1 and ρ_2 are, $\rho_1 = \sqrt{1 - 4m_\pi^2/s}$ and $\rho_2 = \sqrt{1 - 4m_K^2/s}$, respectively. One attempts to extend Eq. (3) down to the lowest threshold. That is, below the second threshold, the above equations may be written as,

$$\text{Im}T_{11} = T_{11}\rho_1 T_{11}^* \,,$$
$$\text{Im}T_{12} = T_{11}\rho_1 T_{12}^* \,,$$
$$\text{Im}T_{22} = T_{21}\rho_1 T_{12}^* \,. \tag{4}$$

But in general Eq. (4) would not be correct in the presence of the anomalous threshold and when the left-hand cut comes across the $4m_\pi^2$ threshold along the real axis. In the present case of $\pi\pi$ and $K\bar{K}$ system there is no anomalous threshold, but the latter does happen. In the $K\bar{K} \to K\bar{K}$ amplitude the left–hand cut starts from $4m_K^2 - 4m_\pi^2$ to $-\infty$. As a consequence the third equation of Eq. (4) only holds true above $4m_K^2 - 4m_\pi^2$ along the real axis rather than above $4m_\pi^2$. The $l.h.c.$ in T_{11} and T_{12} is $(-\infty, 0]$, and $L = (-\infty, 4m_K^2 - 4m_\pi^2]$ for T_{22} (for more information on the location of the $l.h.c.$, see Ref. [30]).

From Eq. (4) the analytic continuation of T or T^I to the second Riemann sheet can be made, [1]

$$T_{11}^{II} = \frac{1}{1 + 2iT_{11}^I\rho_1}T_{11}^I \,,$$
$$T_{12}^{II} = \frac{1}{1 + 2iT_{11}^I\rho_1}T_{12}^I \,,$$
$$T_{22}^{II} = T_{22}^I - 2iT_{21}^I\rho_1 T_{12}^I \frac{1}{1 + 2iT_{11}^I\rho_1} \,, \tag{5}$$

or in short notations,

$$\mathbf{T}^{II} \equiv \mathbf{T}^I \mathbf{B}_{II} = \mathbf{T}^I \begin{pmatrix} \frac{1}{1+2i\rho_1 T_{11}^I} & \frac{-2i\rho_1 T_{12}^I}{1+2i\rho_1 T_{11}^I} \\ 0 & 1 \end{pmatrix} \,. \tag{6}$$

From Eq. (3) one also obtains the T matrix on the third and sequentially on the fourth sheet,

$$\mathbf{T}^{III} \equiv \mathbf{T}^I \mathbf{B}_{III} = \frac{1}{1 + 2i\mathbf{T}^I\rho}\mathbf{T}^I = \mathbf{T}^I \begin{pmatrix} \frac{1+2i\rho_2 T_{22}^I}{\det S} & \frac{-2i\rho_1 T_{12}^I}{\det S} \\ \frac{-2i\rho_2 T_{21}^I}{\det S} & \frac{1+2i\rho_1 T_{11}^I}{\det S} \end{pmatrix} \,, \tag{7}$$

---

[1] We simply point out that, assuming real analyticity, the space between $4m_K^2 - 4m_\pi^2$ and $4m_K^2$ already allows one to make analytic continuation to the second sheet. One may make use of the Källen and Wightman theorem to refine the analysis, but in here we will not discuss the subtlety, the content goes beyond the scope of this paper.

$$\mathbf{T^{IV}} \equiv \mathbf{T^I}\mathbf{B}_{IV} = \mathbf{T^I}\begin{pmatrix} 1 & 0 \\ \frac{-2i\rho_2 T_{21}^I}{1+2i\rho_2 T_{22}^I} & \frac{1}{1+2i\rho_2 T_{22}^I} \end{pmatrix} . \tag{8}$$

Similar discussions on the analytic continuation of the hadron form-factor, $F \equiv (F_1, F_2)$, can also be made. The difference between F and T is that the former is free from left–hand singularities on the physical sheet by construction. The spectral function of F is obtained through the LSZ reduction formalism,

$$\mathrm{Im}F_1 = F_1\rho_1 T_{11}^* + F_2\rho_2 T_{12}^* ,$$
$$\mathrm{Im}F_2 = F_2\rho_2 T_{22}^* + F_1\rho_1 T_{12}^* . \tag{9}$$

The analytic continuation of F is similar to Eqs. (6)–(8),

$$F^{II} = F^I\mathbf{B}_{II} , \quad F^{III} = F^I\mathbf{B}_{III} , \quad F^{IV} = F^I\mathbf{B}_{IV} . \tag{10}$$

The continuation to the fourth sheet can either be obtained by analytic continuation from the second sheet or from the third sheet, which gives of course the same result.

B. The dispersion representation with only left–hand singularities

To proceed we first notice that the method used in Ref. [29] to derive Eq. (1), which requires analyticity of the spectral representation, is not applicable in the coupled–channel situation. For example, one may set up the coupled–channel dispersion integral equation for the form-factor F on the physical sheet (throughout the text dispersion integrals are always written in the un-subtracted form, but possible subtractions are understood),

$$F = \frac{1}{\pi} \int_{4m_\pi^2}^\infty ds' \frac{F(s')\mathbf{K}(s')}{s' - s} , \tag{11}$$

which defines a 2–dimensional singular integral equations with Cauchy kernel, where the integral kernel $\mathbf{K}$, from the above discussion, can be written as,

$$\mathbf{K}(s) = \begin{pmatrix} \rho_1 T_{11}^{II} & \rho_1 T_{12}^{II} \\ 0 & 0 \end{pmatrix}(\theta(s - 4m_\pi^2) - \theta(s - 4m_K^2)) + \begin{pmatrix} \rho_1 T_{11}^{III} & \rho_1 T_{12}^{III} \\ \rho_2 T_{21}^{III} & \rho_2 T_{22}^{III} \end{pmatrix}\theta(s - 4m_K^2) . \tag{12}$$

Apparently, $\mathbf{K}$ is not an analytic function on the real axis even though T is, hence the method in Ref. [29] cannot be used here. Numerical solutions of Eq. (11) are searched for in the literature [28], but the numerical solution is not unique [28] as a reflection of the general mathematical theory [31], and the attempt in picking up the fundamental solution from others becomes extremely difficult numerically.

However, as will be shown in the following, the analytic structure of F defined in Eq. (9) can be studied even though we do not know how to solve Eq. (11) analytically. The crucial observation is that, according to the way of analytic continuation, we have the following identity,

$$\frac{1}{2\pi i}\int_C \{\frac{F_I(\tau)}{\tau - z} + \frac{F_{II}(\tau)}{\tau - z} + \frac{F_{III}(\tau)}{\tau - z} + \frac{F_{IV}(\tau)}{\tau - z}\}d\tau \equiv 0 . \tag{13}$$

5

where the contour C encircles the right–hand cut $R \equiv (4m_K^2 - 4m_\pi^2, \infty)$ and along the contour the complex cut plan is on the left (the contour C would have encircled the entire unitarity cut if there were no l.h.c intercrossed the right–hand cut). Since functions F_I – F_{IV} are analytic on the entire cut plane except for isolated singularities and except for the left–hand cuts the integral contour in Eq. (13) can be deformed, and F can be expressed as sum of poles and left–hand integrals. The form-factor may contain bound state poles on the physical sheet which correspond to the bound state poles of S_I, and may contain resonances from B_{II} to B_{IV} on the other sheets (The virtual state, if exist, can also be incorporated into our formalism easily, but we do not discuss them here for simplicity). The analytic expression of the scalar form-factor on the physical sheet can therefore be obtained,

$$F(z) = \left[\sum \frac{\tilde{F}(s_j)}{z - s_j} \mathbf{C}(s_j) + \sum_{n=II,III,IV} \frac{F(z_i^{(n)}) \tilde{\mathbf{B}}_{(n)}(z_i^{(n)})}{z - z_i^{(n)}} + \frac{1}{2\pi i} \int_L \frac{Disc\,(F\mathbf{C})}{z' - z} dz' \right] / \mathbf{C}(z) ,$$

(14)

where $L = (-\infty, 4m_K^2 - 4m_\pi^2]$. In Eq. (14) s_j denote the positions of bound state poles of F on the physical sheet and z_i^{II}, z_i^{III} and z_i^{IV} denote the position of the resonance poles on the second, third and fourth sheet, respectively. As can be seen from Eqs. (6)– (8), they are also zeros of S_{11}, $\det S$ and S_{22}, respectively. The notations $\tilde{F}$ and $\tilde{\mathbf{B}}$ in the above equation denote the residues of the corresponding functions at their pole positions. The denominator $\mathbf{C}$ in the above equation is,

$$\mathbf{C}(z) \equiv 1 + \mathbf{B}_{II}(z) + \mathbf{B}_{III}(z) + \mathbf{B}_{IV}(z) = \begin{pmatrix} 2 + \frac{1}{S_{11}} + \frac{S_{22}}{\det S} & -2i\rho_1 T_{12}^I \left(\frac{1}{\det S} + \frac{1}{S_{11}} \right) \\ -2i\rho_2 T_{12}^I \left(\frac{1}{\det S} + \frac{1}{S_{22}} \right) & 2 + \frac{1}{S_{22}} + \frac{S_{11}}{\det S} \end{pmatrix} .$$

(15)

Eq. (14) provides an analytic expression of the form-factor F, and the solution of the integral equation (11) provided that the behavior of the form-factor on the left–hand cut is known. However, these formulae are highly non-trivial. Since F_I is free from any left–hand singularity by construction (though F on other sheets does contain the left–hand singularities) and contains no resonance pole on the physical sheet, the residues of F at poles are not free: they have to be arranged in such a way that on the r.h.s. of Eq. (14), the l.h.c. and the zeros in the numerator (the term inside the square bracket) and in the denominator, cancel each other.[2] Though Eq. (14) is rather complicated, one simple way to check the correctness of Eq. (14) is to look at the case when the coupled–channel decouples, that is $T_{21} = T_{12} = 0$. In such a case it is easy to check that the effect of the third sheet is reduced to that of sheet II and IV and,

$$\mathbf{C}(z) = 2 \begin{pmatrix} \frac{1+S_{11}}{S_{11}} & 0 \\ 0 & \frac{1+S_{22}}{S_{22}} \end{pmatrix} .$$

(16)

It is then easy to figure out that Eq. (14) is reduced to two independent single channel expressions [29].

---

[2]The cancellation has only been verified in some very simple cases, see Ref. [29].

In principle, our method presented above can be generalized to the case with more than two coupled–channels, since the key point in deriving the analytic expression, Eq. (13), can be extended to higher dimensional case. Also, Eq. (14) needs more detailed analysis both theoretically and phenomenologically. But we will not discuss these topics here. Instead we will turn to discuss the analytic property of the coupled channel T matrix.

The above method can be easily applied to discuss the analytic structure of the T matrix itself, since the only difference between T and F is that T is itself discontinuous on the left. We have,

$$\frac{1}{2\pi i}\int_C \{\frac{\mathbf{T^I}(\tau)}{\tau - z} + \frac{\mathbf{T^{II}}(\tau)}{\tau - z} + \frac{\mathbf{T^{III}}(\tau)}{\tau - z} + \frac{\mathbf{T^{IV}}(\tau)}{\tau - z}\}d\tau \equiv 0 . \tag{17}$$

from which we get

$$\mathbf{T^I}(z)\,\mathbf{C}(z) + \mathbf{\Phi}(z) - \frac{1}{2\pi i}\int_L \frac{Disc\left(\mathbf{T^I C}\right)}{\tau - z}d\tau = 0 , \tag{18}$$

where

$$(\mathbf{TC})_{11} = \frac{1}{2i\rho_1}\left(S_{11} - \frac{1}{S_{11}} - \frac{S_{22}}{detS} + \frac{detS}{S_{22}}\right) ,$$

$$(\mathbf{TC})_{22} = \frac{1}{2i\rho_2}\left(S_{22} - \frac{1}{S_{22}} - \frac{S_{11}}{detS} + \frac{detS}{S_{11}}\right) ,$$

$$(\mathbf{TC})_{12} = T_{12}\left(1 + \frac{1}{S_{11}} + \frac{1}{S_{22}} + \frac{1}{detS}\right) , \tag{19}$$

and

$$\mathbf{\Phi}(z) = \sum_j \frac{\mathrm{Res}\left[\mathbf{TC}(s_j)\right]}{s_j - z} + \sum_i^{n=II,III,IV} \frac{\mathrm{Res}\left[\mathbf{TC}(z^i_{(n)})\right]}{z^i_{(n)} - z} . \tag{20}$$

In Eq. (20) the first term corresponds to the sum of bound state poles and the bound state may couple to channel 1 or 2, or both. The residues can be read off from Eq. (19). The second sum on the *r.h.s.* of Eq. (20) corresponds to the contribution of resonance poles. It is worth noticing here that not only in $(\mathbf{TC})_{22}$ but also in $(\mathbf{TC})_{11}$ and $(\mathbf{TC})_{12}$ the *l.h.c.* starts from $4m_K^2 - 4m_\pi^2$. One can prove that the matrix function $\mathbf{TC}$ defined in Eq. (19) satisfies the following property,

$$\mathbf{TC}(\rho_1, \rho_2) = \mathbf{TC}(-\rho_1, \rho_2) = \mathbf{TC}(\rho_1, -\rho_2) = \mathbf{TC}(-\rho_1, -\rho_2) . \tag{21}$$

In the case of $\pi\pi$, $K\bar{K}$ scattering we assume there is no bound state pole,[3] so in an explicit form the function $\mathbf{\Phi}$ defined in Eq. (20) can be written as,

---

[3] See however Refs. [11,19,21].

$$\Phi_{11} = -\sum_i \frac{1}{2i\rho_1(z_{II}^i)S_{11}'(z_{II}^i)(z_{II}^i-z)} - \sum_i \frac{S_{22}(z_{III}^i)/2i\rho_1(z_{III}^i)}{(detS)'(z_{III}^i)(z_{III}^i-z)} + \sum_i \frac{detS(z_{IV}^i)/2i\rho_1(z_{IV}^i)}{S_{22}'(z_{IV}^i)(z_{IV}^i-z)}$$

$$\Phi_{22} = \sum_i \frac{detS(z_{II}^i)/2i\rho_2(z_{II}^i)}{S_{11}'(z_{II}^i)(z_{II}^i-z)} - \sum_i \frac{S_{11}(z_{III}^i)/2i\rho_2(z_{III}^i)}{(detS)'(z_{III}^i)(z_{III}^i-z)} - \sum_i \frac{1}{2i\rho_2(z_{IV}^i)S_{22}'(z_{IV}^i)(z_{IV}^i-z)}$$

$$\Phi_{12} = \sum_i \frac{T_{12}^I(z_{II}^i)}{S_{11}'(z_{II}^i)(z_{II}^i-z)} + \sum_i \frac{T_{12}^I(z_{III}^i)}{(detS)'(z_{III}^i)(z_{III}^i-z)} + \sum_i \frac{T_{12}^I(z_{IV}^i)}{S_{22}'(z_{IV}^i)(z_{IV}^i-z)} \ . \tag{22}$$

C. The analytic property of the function TC

A question naturally arise at this moment is that what we have done by transforming the matrix $\mathbf{T}$ to $\mathbf{TC}$ as expressed by Eq. (19)? The answer is of course that under such a transformation the matrix function $\mathbf{TC}$ is real analytic on R. The imaginary part of $\mathbf{TC}$ in the region $(4m_\pi^2, 4m_K^2 - 4m_\pi^2)$ comes solely from the dynamical effects of the *l.h.c.*, as $\mathbf{TC}(\rho_1, \rho_2) = \mathbf{TC}(-\rho_1, \rho_2)$ in this region. To see this more clearly one may perform a perturbation expansion, for example a chiral expansion, on $\mathbf{TC}$. Up to $O(p^4)$ term, one may write,

$$(\mathbf{TC})_{11} = \frac{1}{2i\rho_1}\left(8i\rho_1(T_{11}^{(2)} + T_{11}^{(4)}) + 8\rho_1^2 T_{11}^{(2)2} + 8\rho_1\rho_2 T_{12}^{(2)}T_{21}^{(2)}\right) + O(p^6) \ , \tag{23}$$

where the superscripts in the small brackets denote the order of chiral expansion in powers of p^2. Along the real axis above the second threshold, one can use the perturbation unitarity relation to recast Eq. (23) as,

$$(\mathbf{TC})_{11} = 4\mathrm{Re}T_{11}^{(2)+(4)} + O(p^6) \tag{24}$$

which is indeed real. Below the second threshold but above the first threshold one uses the first equation in Eq. (4) and obtains,

$$(\mathbf{TC})_{11} = 4\mathrm{Re}T_{11}^{(2)+(4)} - 4i\rho_2 T_{12}^{(2)}T_{21}^{(2)} + O(p^6) \ , \tag{25}$$

which is again real analytic. One should not draw a conclusion from Eq. (25) that $(\mathbf{TC})_{11}$ is real analytic down to $4m_\pi^2$. A close look at Eq. (19) reveals that $(\mathbf{TC})_{11}$ contains the *l.h.c.* up to $4m_K^2 - 4m_\pi^2$ which comes from sheet III and sheet IV of the Riemann surface defined by the S matrix, but these cuts do not show at order $O(p^4)$. In fact, it is straightforward to check the appearance of the *l.h.c.* when we expand $(\mathbf{TC})_{11}$ to $O(p^8)$,

$$\begin{aligned}
(\mathbf{TC})_{11} = {} & 4T_{11} - 4i(\rho_1 T_{11}^2 + \rho_2 T_{12}T_{21}) - 8(\rho_1^2 T_{11}^3 + \rho_1\rho_2 T_{11}T_{12}T_{21} + \rho_2^2 T_{12}T_{22}T_{21}) \\
& + 8i(2\rho_1^3 T_{11}^4 + 3\rho_1^2\rho_2 T_{11}^2 T_{12}T_{21} + 2\rho_1\rho_2^2 T_{11}T_{12}T_{22}T_{21} + T_{12}T_{21}\rho_2^2(T_{12}T_{21}\rho_1 + 2T_{22}^2\rho_2)) \\
& + O(p^{10}) \ .
\end{aligned} \tag{26}$$

The *l.h.c.* contribution firstly shows in the third term inside the second bracket on the *r.h.s.* of the above equation. The lowest order contribution it contains is $\sim O(p^4)\mathrm{Im}T_{22}$. It is easily understood that this term can not be cancelled by sequential terms in the chiral expansion since the latter are at least of order of $O(p^6)\mathrm{Im}T_{22}$.

For $(\mathbf{TC})_{22}$ we have

$$(\mathbf{TC})_{22} = \frac{1}{2i\rho_2}\left(8i\rho_2 T_{22}^{(2)+(4)} + 8\rho_2^2 T_{22}^{(2)2} + 8\rho_1\rho_2 T_{12}^{(2)} T_{21}^{(2)}\right) + O(p^6) , \qquad (27)$$

which is equally well written as

$$(\mathbf{TC})_{22} = 4\mathrm{Re}T_{22}^{(2)+(4)} + O(p^6) \qquad (28)$$

above the second threshold, and

$$(\mathbf{TC})_{22} = 4\mathrm{Re}T_{22}^{(2)+(4)} - 4i\rho_2 T_{22}^{(2)2} + 4i(\mathrm{Im}T_{22}^{(4)} - \rho_1 T_{12}^{(2)} T_{21}^{(2)})O(p^6) \qquad (29)$$

when $s < 4m_K^2$. The difference between here and the 11 channel is that in here the *l.h.c.* already appears in the physical sheet defined by S. For completeness we also list result for $(\mathbf{TC})_{12}$,

$$(\mathbf{TC})_{12} = 4(T_{12}^{(2)} + T_{12}^{(4)}) - 4i(\rho_1 T_{11}^{(2)} T_{12}^{(2)} + \rho_2 T_{12}^{(2)} T_{22}^{(2)}) + O(p^6) \qquad (30)$$

and the *r.h.s.* is equal to $4\mathrm{Re}T_{12}^{(2)+(4)} + O(p^6)$ when $s > 4m_K^2$ and equals to $4\mathrm{Re}T_{12}^{(2)+(4)} - 4i\rho_2 T_{12}^{(2)} T_{22}^{(2)} + O(p^6)$ when $4m_K^2 - 4m_\pi^2 < s < 4m_K^2$.

From the above discussion it is realized that $(\mathbf{TC})_{11}$ indeed contains a left–hand branch point singularity at $s = 4m_K^2 - 4m_\pi^2$. The perturbative expansion is just used for pedagogical reasons. Of course the chiral expansion is badly violated in the energy region around the $K\bar{K}$ threshold, and the perturbative results should not be used to argue in favor of the smallness of the left–hand cut contributions.

It is also helpful to understand more about the property of the function $\mathbf{TC}$ by examining how it behaves in some simple models. For example in a simple Breit–Wigner narrow resonance model, one may construct the S matrix satisfying unitarity:

$$\begin{aligned}
T_{11} &= \frac{e^{2i\phi} - 1}{2i\rho_1} + \frac{g_1 e^{2i\phi}}{M_R^2 - s - i(\rho_1 g_1 + \rho_2 g_2)} , \\
T_{12} &= \frac{\sqrt{g_1 g_2} e^{i\phi}}{M_R^2 - s - i(\rho_1 g_1 + \rho_2 g_2)} , \\
T_{22} &= \frac{g_2}{M_R^2 - s - i(\rho_1 g_1 + \rho_2 g_2)} ,
\end{aligned} \qquad (31)$$

where g_1, g_2 are coupling constants and M_R is the bare mass parameter. In this model the background phase is simulated by the function $\phi(s)$ with

$$e^{i\phi} = \frac{\alpha(s) + i\rho_1\beta(s)}{\alpha(s) - i\rho_1\beta(s)} , \qquad (32)$$

in which $\alpha(s)$ and $\beta(s)$ are real polynomials. It is easy to verify that the background phase as defined in Eq. (32) obeys the requirement of real analyticity.

The T matrix defined by Eq. (31) contains both the *l.h.c.* (from 0 to $-\infty$) and the right–hand cuts, due to the presence of the kinematic factors. However a simple algebraic calculation reveals that the function TC is a matrix of real rational functions, that is, it is

9

analytic on the entire s plane with only isolated singularities. In this sense the structure of the S matrix defined by Eqs. (31) and (32) is topologically trivial. This observation, which follows from Eq. (21) also applies to more general case of the K matrix parametrization when K takes the form of rational functions. Though topologically trivial, simple models as discussed above can still be helpful in revealing the qualitative picture of the $\pi\pi$ and $K\bar{K}$ coupled–channel system.

III. THE ANALYTIC STRUCTURE OF $\pi\pi$ AND $K\bar{K}$ COUPLED–CHANNEL SYSTEM: THE TWO δ_πS

A. The $\pi\pi$ scattering phase in coupled–channel unitarity region

In the physical region above the second threshold, there is the well known parametrization of the scattering S matrix,

$$S = \begin{pmatrix} \eta e^{2i\delta_\pi}, & i\sqrt{1-\eta^2}e^{i(\delta_\pi+\delta_K)} \\ i\sqrt{1-\eta^2}e^{i(\delta_\pi+\delta_K)}, & \eta e^{2i\delta_K} \end{pmatrix} . \tag{33}$$

By using it Eq. (19) can be recasted as

$$
\begin{aligned}
(\mathbf{TC})_{11} &= \frac{1}{\rho_1}\frac{\eta^2+1}{\eta}\sin 2\delta_\pi \ , \\
(\mathbf{TC})_{22} &= \frac{1}{\rho_2}\frac{\eta^2+1}{\eta}\sin 2\delta_K \ , \\
(\mathbf{TC})_{12} &= \frac{(1-\eta^2)^{\frac{1}{2}}}{\sqrt{(\rho_1\rho_2)}}\left(\cos(\delta_\pi+\delta_K)+\frac{1}{\eta}\cos(\delta_\pi-\delta_K)\right) \ ,
\end{aligned}
\tag{34}
$$

and from Eq. (18) we obtain,

$$\sin 2\delta_\pi = -\frac{\eta}{1+\eta^2}\rho_1\left(\Phi_{11}(s)-\frac{1}{2\pi i}\int_L \frac{Disc\left(\mathbf{T^I C}\right)_{11}}{z-s}dz\right) \ ,$$

$$\sin 2\delta_K = -\frac{\eta}{1+\eta^2}\rho_2\left(\Phi_{22}(s)-\frac{1}{2\pi i}\int_L \frac{Disc\left(\mathbf{T^I C}\right)_{22}}{z-s}dz\right) \ ,$$

$$\cos(\delta_\pi+\delta_K)+\frac{1}{\eta}\cos(\delta_\pi-\delta_K) = -\frac{\sqrt{\rho_1\rho_2}}{(1-\eta^2)^{\frac{1}{2}}}\left(\Phi_{12}(s)-\frac{1}{2\pi i}\int_L \frac{Disc\left(\mathbf{T^I C}\right)_{12}}{z-s}dz\right) \ . \tag{35}$$

In above equations the function $\mathbf{\Phi}$ is a rational function with real coefficients and the left hand integrals are also real analytic functions due to the property of real analyticity of the T matrix and $L = (-\infty, 4m_K^2 - 4m_\pi^2]$.

It is convenient to read from Eq. (35) that $\sin(2\delta_\pi)$ as an analytic function on the entire physical sheet, after analytic continuation, contains the *l.h.c.* starting from $4m_K^2 - 4m_\pi^2$ to the left of the real axis. It is easy to understand that $\sin(2\delta_\pi)$ and η have this *l.h.c.* separately in such a way that the *l.h.c.* starting from $4m_K^2 - 4m_\pi^2$ in their combination, S_{11},

cancels. The appearance of such a *l.h.c.* can be clearly seen from the following expressions for $\sin(2\delta_\pi)$ and η which are appropriate for the analytic continuation,

$$\sin(2\delta_\pi) \equiv \rho_1 \mathcal{F}_2 = \frac{1}{2i}(\frac{1}{\eta}S_{11} - \frac{1}{S_{11}}\eta) \ , \tag{36}$$

$$\eta = \sqrt{S_{11}S_{22}/detS} \ , \tag{37}$$

from which we read off,

$$\mathcal{F}_2^{III} = \mathcal{F}_2^I \ , \quad \eta^{III} = \eta^I \ , \tag{38}$$

and

$$\mathcal{F}_2^{II} = \mathcal{F}_2^I \ , \quad \eta^{II} = 1/\eta^I \ , \tag{39}$$

which are correct when Eq. (3) and Eq. (4) are correct, respectively. From these properties it is realized that on the real axis $\mathcal{F}_2$ only contains the *l.h.c.*, and η only contains the cut in the region $[4m_K^2 - 4m_\pi^2, 4m_K^2]$ (where η is a pure phase) and the *l.h.c.* on the left. These look good at first glance for setting up dispersion relations for these quantities. But η contains many branch point singularities (and so does $\sin(2\delta_\pi)$) on the complex s plane (corresponding to the positions of resonance poles), which prevent the usefulness of these dispersion relations.

In another combination of η and $\sin(2\delta_\pi)$ which appears in the first equation of Eq. (34), as we demonstrated before, the right–hand cuts cancel. Eq. (35) is the appropriate one for phenomenological discussions, as similar to the single channel case [29]. For example, one may use the experimental data of δ_π, δ_K and η in the region above the $K\bar{K}$ threshold to study the properties of the widely concerned $f_0(980)$ resonance. Unfortunately, the left–hand integrals in the energy region required by coupled–channel analysis are very difficult to estimate theoretically. [4] This shortcoming limits the phenomenological usage of our method. But our approach can still be helpful in studying the coupled–channel system, as will be discussed in Sec. IV.

B. The $\pi\pi$ scattering phase in single channel unitarity region

The analytic structure of the $\pi\pi$ phase shift defined in the coupled–channel unitarity region (denoted as $\delta_\pi^{(2)}$ later on) is remarkably different from the analytic structure of δ_π defined in the single channel unitarity region (denoted as $\delta_\pi^{(1)}$ hereafter):

$$\sin(2\delta_\pi^{(1)}) \equiv \rho_1 \mathcal{F} = \frac{1}{2i}(S_{11} - 1/S_{11}) \ . \tag{40}$$

The function $\mathcal{F}$ defined in above equation only contains the left–hand cut starting from $s = 0$ together with the ordinary unitarity cut starting from $4m_K^2$. It now becomes clear

---

[4]The perturbation expansion fails badly here, and the matrix Padé approximation destroys the single channel unitarity of the $\pi\pi$ amplitude by giving it the *l.h.c.* on the physical sheet [1,32].

that the two δ_π are not analytic continuation to each other though they match at $s = 4m_K^2$. One can then set up a dispersion relation for $\mathcal{F}$,

$$\mathcal{F}(s) = \sum_i \frac{Res[\mathcal{F}(z_i^{II})]}{s - z_i^{II}} + \frac{1}{\pi}\int_{-\infty}^0 \frac{\text{Im}_L\mathcal{F}}{s' - s}ds' + \frac{1}{\pi}\int_{4m_K^2}^\infty \frac{\text{Im}_R\mathcal{F}}{s' - s}ds' \ , \qquad (41)$$

where the poles are only from the second sheet in the absence of bound state poles. Eq. (41) is the extension of the single channel result [29] in the coupled–channel case. Comparing with Eq. (42) of Ref. [29] only the third term is new and the other two terms are the same. The first integral on the r.h.s. of Eq. (41) has been discussed at length in Ref. [29], and it is fortunate that the second integral on the r.h.s. of Eq. (41) can be estimated from experiments since

$$\text{Im}_R\mathcal{F} = \frac{1}{2}(1/\eta - \eta)\cos(2\delta_\pi^{(2)}) \qquad (42)$$

in the coupled–channel region.

IV. PHENOMENOLOGY OF THE COUPLED–CHANNEL DISPERSION RELATIONS

A. The $f_0(980)$ pole and the nearby singularities

From Eq. (41) we see that when s approaches $4m_K^2$ from the lower side the value of the right integral will change rapidly since $s = 4m_K^2$ is its branch point. It is well known that the branch point will develop a cusp structure to the real part of the dispersive integral. Also we see in the above subsection that $\sin(2\delta_\pi^{(2)})$ contains a left–hand branch point at $4m_K^2 - 4m_\pi^2$. Both of the two branch point singularities are *very* close to the pole position of the $f_0(980)$ resonance. Therefore it is necessary to carefully investigate the influence of the branch point singularities to the determination of the pole position. In a typical K matrix fit dynamical singularities rather than poles are simulated by background polynomials. However the cusp structure of the branch point singularity should not be well simulated by a smooth background polynomial, especially when the background polynomial is being used to cover a large region of s. It is even reasonable to imagine whether such a cusp phenomenon could be responsible for the sharp rise of $\delta_{\pi\pi}$ near the $K\bar{K}$ threshold.[5] However, a numerical estimate to the right–hand integral in Eq. (41) indicates that the right–hand cut effect is very weak. In Fig. 1 we plot the right–hand integral contribution to $\mathcal{F}$ from two fits found in the literature [2,6], here the integration is performed from the $K\bar{K}$ threshold to roughly about $\sqrt{s} \simeq 1.5$ GeV. As we see from Fig. 1 that the contribution of the right–hand integral is in the right direction to increase $\sin(2\delta_\pi^{(1)})$ rather rapidly, but the effect is too small to have any non-negligible influence to the $f_0(980)$ pole. This can be clearly seen by comparing

---

[5]It is very impressive to notice that in Ref. [2], it was carefully tested up to 40 parameters in the background phase to check whether the background polynomial can be responsible for such a sharp rise.

Fig 1 with Fig 2. In the latter case $\sin(2\delta_\pi)$ jumps from -1 to +1 near the $K\bar{K}$ threshold whereas the contribution from the right–hand integral is one order of magnitude smaller. When estimating the right–hand integral we make use of Eq. (42) which assumes implicitly two–channel unitarity. Though the two–channel unitarity no longer holds true when the 4π channel and the $\eta\eta$ channel become important, we expect the order of magnitude estimate remains valid.

The left–hand integrals appeared in the coupled–channel equations, though can not be estimated quantitatively, can also be proven to behave mildly when the narrow $f_0(980)$ resonance is located on the second sheet (see Eq. (46) and related discussions).

B. A combined fit of the coupled–channel and the single channel equations

The single channel dispersion relation, Eq. (41) contains only the second sheet pole whereas the coupled–channel equations, Eq. (35) contain resonance poles on all sheets, i.e., sheet II, III and sheet IV. In the single channel approximation [29] we have to introduce 4 parameters for each resonance pole, two of them are related to the pole position and the another two are related to the residue, or the resonance coupling to $\mathcal{F}$. Now in the coupled–channel case each resonance pole contains 6 parameters, two of them are for the pole position, two are for the resonance coupling to $\mathcal{F}$ (for second sheet poles only) and/or Φ_{11} (the second sheet pole coupling to $\mathcal{F}$ and Φ_{11} are the same), and the last two are for the coupling in Φ_{22}. The pole coupling in Φ_{12} is not independent as can be verified from Eq. (22). It is annoying to have so many parameters associated with a resonance pole. These parameters are in principle correlated to each other, but no simple relation with stringent constraint between these terms are found. Therefore in here we approximate these parameters as uncorrelated in the fit. However the property of the $f_0^{II}(980)$ narrow resonance obtained under such an approximation is expected not distorted much from the real situation, since the sharp rise of the $\pi\pi$ scattering phase near the $K\bar{K}$ threshold is so deterministic, as can be seen from the following discussions.

In the $\pi\pi$ and $K\bar{K}$ coupled–channel system, following the conventional wisdom, we assume two second sheet poles. One corresponds to the σ resonance, the another corresponds to the $f_0(980)$ resonance, in addition we assume there exists another 3rd sheet pole which simulate all other pole contributions.[6] The right–hand integral is estimated using that depicted in Fig. 1 which is however found to have only tiny influence. We estimate the left–hand integral in Eq. (41) in the same way as in Ref. [29]. That is we either use χPT to evaluate $\mathrm{Im}\mathcal{F}_L$ but with a truncated integral interval at $-\Lambda^2$ (here we take $\Lambda= 600\mathrm{MeV}$, $700\mathrm{MeV}$, $800\mathrm{MeV}$ and $1\mathrm{GeV}$), or estimate $\mathrm{Im}\mathcal{F}_L$ from the [1,1] Padé solution. [7]

---

[6]A shortcoming of the present method is that we can not distinguish the third sheet pole from the fourth sheet pole in Eq. (35).

[7]We are not able to estimate the left hand cut at quantitative level. In a previous version we had fixed $\mathrm{Im}\mathcal{F}_L$ using the Padé approximant, but then we realized the problem associated with the Padé approximation [33]. Fortunately the pole positions of the σ and the $f_0(980)$ resonances are

In the coupled–channel unitarity region, or in Eq. (35), however, we do not have a reliable method to estimate the left–hand integrals. We therefore simulate them by a group of (totally 3) polynomials. In here we restrict ourselves in a modest range of energy region, $2m_K < \sqrt{s} < 1.2GeV$, therefore the polynomials may take simple and smooth forms, i.e., constants or linear polynomials which further introduce a few more parameters. In the absence of narrow 3rd or 4th sheet pole close to the branch point singularity at $4m_K^2 - 4m_\pi^2$ the validity of this approximation can be justified. Furthermore, the matching condition,

$$\sin(2\delta_\pi^{(1)})|_{s=4m_K^2} = \sin(2\delta_\pi^{(2)})|_{s=4m_K^2} \tag{43}$$

is used to reduce one parameter in the $\pi\pi$ channel.

In the single channel unitarity region we use the combination of the CERN–Munich data and the low energy data from K_{e4} decay [34], and especially the new experimental data from the E865 Collaboration [35]. We take the K meson mass to be $m_K = (m_{K^\pm} + m_{K_s})/2$ in our fit. In the coupled–channel unitarity region we use the experimental data on $\delta_\pi + \delta_K$ and $(1 - \eta_{00}^2)/4$ from Refs. [36,37], and the data on δ_π from Refs. [38,39].[8] In order to extract the "experimental" value of **TC** in the coupled–channel unitarity region we have to shift the data to same points of s by proper extrapolation. With such a manipulation to the data, we are able to make the fit, see Fig. 2 and Figs. 3–5 for a typical example of the fit where the left–hand integrals in the coupled–channel equations are approximated by constants. In the fit we find that, even for a very simple parametrization form of the left–hand integral, there may exist different solutions – the position of the 'third sheet pole' is found to be very unstable. This even occurs when the 3rd sheet pole is correlated to the 2nd sheet pole via a Breit–Wigner narrow resonance model like that in Eq. (31). In the uncorrelated case the solutions for the 3rd (or 4th) sheet pole is quite arbitrary: The mass roughly ranges from $0.7 \sim 1.2$GeV and the width ranges from very small values to roughly about 0.6GeV. This uncertainty may be partly due to the unsatisfactory quality of the manipulated data in the coupled–channel unitarity region (see Figs. 3–5), but it is amazing to notice that such an uncertainty for the 3rd/4th sheet pole does exist in the literature where very different solutions are also found (see the compilation of the 2000 edition of the Review of Particle Physics [27] for more information). Irrespective of the large uncertainty that the 3rd/4th sheet pole has, the σ pole position and the f_0^{II} pole position are however found to be rather stable against changes of the parametrization form of cuts and the uncertainties related to the first left hand cut. The results are summarized in what follows:

$$M_\sigma = 450 \sim 510\text{MeV} \ , \ \ \Gamma_\sigma = 480 \sim 550\text{MeV} \ ;$$
$$M_{f_0^{II}} = 981 \sim 992MeV \ , \ \ \Gamma_{f_0^{II}} = 32 \sim 40\text{MeV} \ ;$$
$$a_0^0 \ = 0.24 \sim 0.27 \ . \tag{44}$$

Very similar to the what happens in the single–channel situation [29], the location of the σ resonance is sensitive to the choice of the scattering length used in the fit. If the χPT result

---

found not sensitive to the uncertainties related to our different choices of the left hand cut.

[8]Such a choice of data set merely reflects our prejudice by excluding the results of Refs. [40,41].

of $a_0^0 = 0.220 \pm 0.005$ [42] is used as a constraint in the fit we find instead the following results (here we take the Padé solution of the first left hand cut for example):

$$M_\sigma = 465 \sim 468\text{MeV} \ , \ \ \Gamma_\sigma = 610 \sim 650\text{MeV} \ ;$$
$$M_{f_0^{II}} = 981 \sim 983 MeV \ , \ \ \Gamma_{f_0^{II}} = 31 \sim 33\text{MeV} \ ;$$
$$a_0^0 \simeq 0.221 \ . \tag{45}$$

From the results list above we find that the pole position of the $f_0(980)$ resonance is very stable. Furthermore the inclusion of the $f_0^{II}(980)$ pole has only modest influence to the pole position of the σ resonance by comparing with the results from Ref. [29].[9] The main reason of the stability is due to the special data point in the upper right region in Fig. 2 from the CERN–Munich data: $\sqrt{s} = 0.99\text{GeV}$ with the value of $\delta_\pi = 234.0 \pm 12.3$ degrees. The center of mass energy of this data point already exceeds $2m_{K^\pm}$ though it is located below the $K^0\bar{K}^0$ threshold. In our fit we set the K meson mass as $m_K = (m_{K^\pm} + m_{K_s})/2$ which is above 0.99GeV, so we count this point in the single channel unitarity region (notice that this data point is very close to $2m_{K^\pm}$). Also considering the experimental error bar for the beam energy, the location and the value of this data point contributes the major uncertainty in the determination of the location of the $f_0(980)$ resonance (mainly affects the width). Manifestly our approach is sensitive to the experimental data near the $K\bar{K}$ threshold region. On the qualitative level, however, the picture that there exists a very narrow $f_0(980)$ pole on the second sheet should not be altered, as is determined unambiguously by the fact that the value of $\sin(2\delta_\pi)$ at the matching point (see Eq. (43)) is much closer to $+1$ rather than to -1.

C. The subtlety in our approach: if the $f_0(980)$ narrow resonance does not locate on the second sheet

As pointed out in the above subsection that the data point closest to the $K\bar{K}$ threshold is crucial in determining a narrow resonance on the second sheet, named as the $f_0^{II}(980)$. One has to be very cautious under such a situation when the fit is very sensitive to a single data point. For example, if this point were removed from the data in fitting Eq. (41), or in other words if the value of $\sin(2\delta_\pi)$ at the matching point (see Eq. (43)) is closer to -1 rather than to $+1$, the fit program would prefer a solution without the narrow second sheet pole. Instead, it would give a solution roughly at $M_{f_0^{II}} \sim 0.86\text{GeV}$ and $\Gamma_{f_0^{II}} \sim 0.16\text{GeV}$ and a very narrow third (or 4th) sheet pole, $M \sim 0.96 - 0.98\text{GeV}$ and $\Gamma \sim 5 - 35\text{MeV}$. Under such a circumstance it is the 3rd (or 4th) sheet pole combing with the *l.h.c.* in the first equation in Eq. (35), rather than the narrow second sheet pole, being mainly responsible for the sharp rise of the $\pi\pi$ phase shift *above* the $K\bar{K}$ threshold. Though rather academic, it is worth pointing out that if such a scenario would happen the narrow pole position could not be reliably estimated within the present approach, because the third (or 4th) sheet pole will have a very strong influence to the left–hand integrals in the coupled–channel dispersion equations. To make the point more clear let us write down the following formula,

---

[9]Previous results on this point can be found in Refs. [43,44].

$$\frac{1}{2i}Disc(\mathbf{TC}_{11}) = -4\rho_2^2\Delta_{lhc}\frac{|T_{12}|^2}{S_{22}detS^*} + h.c. \ , \tag{46}$$

where Δ_{lhc} is defined as

$$\mathrm{Im}T_{22} = \rho_1|T_{12}|^2 + \Delta_{lhc}\theta(4m_K^2 - 4m_\pi^2 - s) \ , \tag{47}$$

in the single channel unitarity region. We have no knowledge on how to estimate Δ_{lhc} and we assume it behaves normally in the sense that its order of magnitude and the behavior is similar to, say, the *l.h.c.* appeared in the single channel equation. Then it is apparently shown in the above formula that a very narrow resonance on the 3rd or 4th sheet near the left–hand branch point at $s = 4m_K^2 - 4m_\pi^2$ will greatly enhance the discontinuity of $\mathbf{TC}_{11}$ and also the cusp structure of the dispersion integral of $\mathbf{TC}_{11}$ provided that the sign is correct (*i.e.*, to give a sharp rise, not a sharp decrease, to $\sin(2\delta_\pi^{(2)})$). The 3rd or 4th sheet pole itself would also contribute in Eq. (35) (but not in Eq. (41)), a combined contribution of the cut and the pole may therefore explain the sharp rise of $\sin(2\delta_\pi^{(2)})$. But of course such a scenario is unambiguously excluded by experiments.

V. CONCLUSION

In this paper we have studied the IJ=00 $\pi\pi$ and $K\bar{K}$ coupled–channel system by using dispersion relations which are set up after a careful analysis to the analytic structure of the coupled–channel system. The effects of various cuts on the determination of pole positions are discussed and estimated which are found to be mild in general. Especially the role of the left hand cut starting from $4m_K^2 - 4m_\pi^2$ is clarified. Especially, the cut has little influence to the determination of second sheet poles.

We therefore confirm, at qualitative level, the conventional wisdom in the widely used K matrix fit to simulate these dynamical singularities by mild background polynomials. To some extent, our analysis also justifies the dynamical assumption made in dynamical approaches (see for example, Refs. [45,46]) to partly neglect the t channel exchange forces by assuming them to behave mildly.

We conclude from the discussion in this paper that there exists a very narrow second sheet pole with mass about $981 \sim 992$MeV and width about $32 \sim 40$MeV which is responsible for the sharp increase of the $\pi\pi$ scattering phase near (mainly below) the $K\bar{K}$ threshold. Meanwhile the mass and the width of the σ resonance is estimated to be $M_\sigma = 450 \sim 510$MeV, $\Gamma_\sigma = 480 \sim 550$MeV. However, we pointed out that the width of the narrow second sheet pole is sensitive to the data near the $K\bar{K}$ threshold, and therefore future experiments with more accurate data are called for. We also find that the possible third sheet pole which is related to the narrow second sheet pole in the coupled channel Breit–Wigner resonance model can not be reliably fixed at present stage within our scheme. The reason is simply because only the data above the $K\bar{K}$ threshold can contribute to the determination of the third sheet pole and also the left hand cut starting from $4m_K^2 - 4m_\pi^2$ pollutes here.

Our results on the pole locations of the σ and f_0^{II} resonances are in qualitative agreement with the results found in the literature, though the method used in this paper is rather different from those commonly used. In our opinion, the IJ=00 $\pi\pi$ and $K\bar{K}$ coupled–channel system is so interesting and important and it is always meaningful to study it from

16

different angles which can bring us more understanding and insight in the related physics. Our method may be generalized to others channels as well. But the dynamical singularities appeared in the case of unequal mass scatterings are more complicated. For example, in the case of πK scattering we will run into the more complicated problem of dealing with the circular cut.

REFERENCES

[1] D. Iagolnitzer, J. Zinn-Justin and J. B. Zuber, Nucl. Phys. **B60**, 233(1973).

[2] K. L. Au, D. Morgan and M. R. Pennington, Phys. Rev. **D35**, 1633(1987).

[3] M. Aguilar-Benitez *et al.*, Z. Phys. **C50**, 405(1991).

[4] T. A. Armstrong *et al.*, Z. Phys. **C51**, 351(1991).

[5] D. Morgan and M. R. Pennington, Phys. Rev. **D48**, 1185(1993).

[6] B. S. Zou, B. V. Bugg, Phys. Rev. **D50**, 591(1994).

[7] R. Kaminski *et al.*, Phys. Rev. **D50**, 3145(1994).

[8] D. V. Bugg *et al.*, Phys. Rev. **D50**, 4412(1994).

[9] V. V. Anisovich *et al.*, Phys. Lett. **B323**, 233(1994).

[10] C. Amsler *et al.*, Phys. Lett. **B333**, 277(1994).

[11] G. Janssen *et al.*, Phys. Rev. **D52**, 2690(1995).

[12] V. V. Anisovich *et al.*, Phys. Lett. **B355**, 363(1995).

[13] C. Amsler *et al.*, Phys. Lett. **B355**, 425(1995); **B342**, 433(1995).

[14] D. M. Alde *et al.*, Z. Phys. **C66**, 375(1995).

[15] N. A. Tornqvist and M. Roos, Phys. Rev. Lett. **76**, 1575(1996).

[16] S. Ishida *et al.*, Prog. Theor. Phys. **95**, 745(1996).

[17] A. Bertin *et al.*, Phys. Lett. **B408**, 476(1997).

[18] N. N. Achasov *et al.*, Phys. Rev. **D56**, 4084(1997).

[19] M. Locher, V. Markushin and H. Zheng, Euro. Phys. J. **C4**, 317(1998).

[20] J. A. Oller and E. Oset, Phys. Rev. **D60**, 074023(1999).

[21] J. A. Oller and E. Oset, Nucl. Phys. **A652**, 407(1999).

[22] J. A. Oller *et al.*, Phys. Rev. **D60**, 099906(1999).

[23] R. Kaminski, L. Lesniak and B. Loiseau, Euro. Phys. J. **C9**, 141(1999).

[24] M. Boglione and M. R. Pennington, Euro. Phys. J. **C9**, 11(1999).

[25] D. Barberis *et al.*, Phys. Lett. **B462**, 462(1999).

[26] Yu. S. Surovtsev, D. Krupa and M. Nagy, Acta Phys. Polon. B31 (2000) 2697.

[27] Review of Particle Physics, Eur. Phys. J. C15 (2000) 1.

[28] W. Liu, H. Q. Zheng and X. L. Chen, Commun. Theor. Phys. **35** (2001) 543.

[29] Z. Xiao and H. Q. Zheng, hep-ph/0011260, to appear in Nucl. Phys. A.

[30] J. Kennedy and T. D. Spearman, Phy. Rev. **126**, 1596 (1962).

[31] N. I. Muskhelishvili, *Singular Integral Equations*, (Moscow, 1946); J. K. Lu, *Boundary value problems for analytic functions* World Scientific, Singapore, 1993.

[32] F. Guerrero and J. A. Oller, Nucl. Phys. **B537** (1999) 459.

[33] Q. Ang, Z. G. Xiao, H. Zheng and X. C. Song, hep-ph/0109012, submitted to Commun. Theor. Phys..

[34] L. Rosselet *et al.*, Phys. Rev. **D15** (1977) 574.

[35] P. Truoel *et al.* (E865 Collaboration), hep-ex/0012012.

[36] D. Cohen, Phys. Rev. **D22**, 2595(1980).

[37] A. D. Martin and E. N. Ozmuth, Nucl. Phys. **B158**, 520(1979).

[38] G. Grayer et al., Proc. 3rd Philadelphia Conf. on Experimental Meson Spectroscopy, Philadelphia, 1972 (American Institute of Physics, New York, 1972) 5.

[39] B. Hyams et al., Nucl. Phys. B64, 134(1973).

[40] S. J. Lindenbaum *et al.*, Phys. Lett. **B274**, 492(1994).

[41] C. D. Froggatt *et al.*, Nucl. Phys. **B129**, 89(1977).

[42] G. Colangelo, J. Gasser and H. Leutwyler, hep-ph/0103088.

[43] A. Dobado and J. R. Pelaez, Phys. Rev. **D56** 3057 (1997).

[44] J. A. Oller, E. Oset, J. R. Pelaez, Phys. Rev. **D59** 074001 (1999); Erratum *ibid.* **D60** 099906 (1999).

[45] J. A. Oller and E. Oset, Nucl. Phys. **A620** 438 (1997); Erratum *ibid.* **A652** 407 (1999).

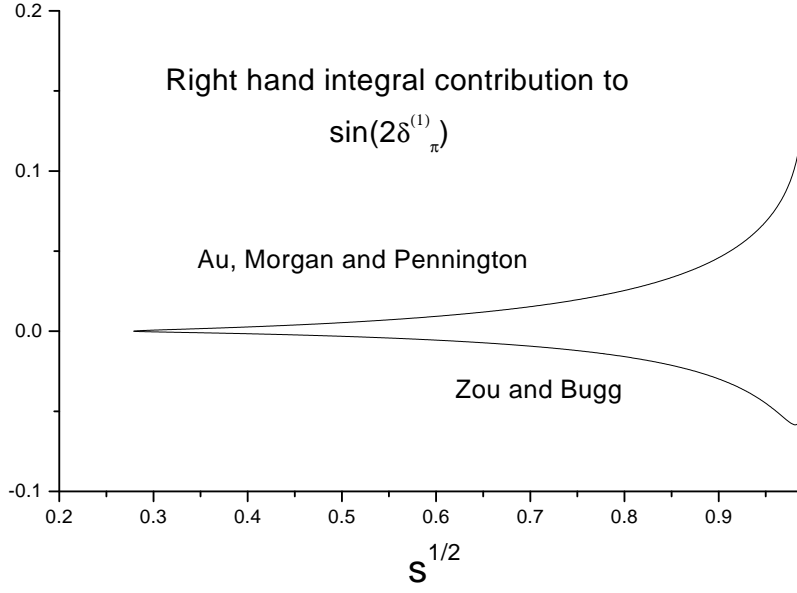[46] V. E. Markushin, Eur. Phys. J. **A8** 389 (2000).

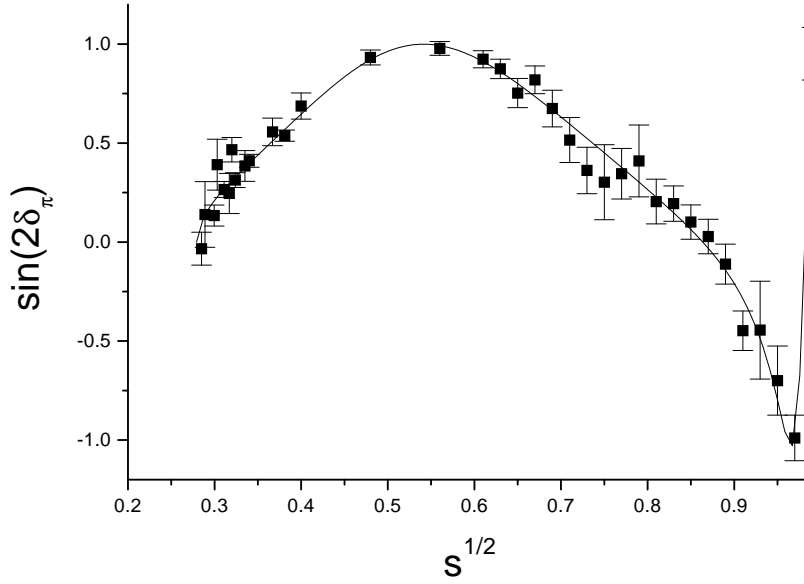FIG. 1. The contribution from the right–hand integral to $\mathcal{F}$.

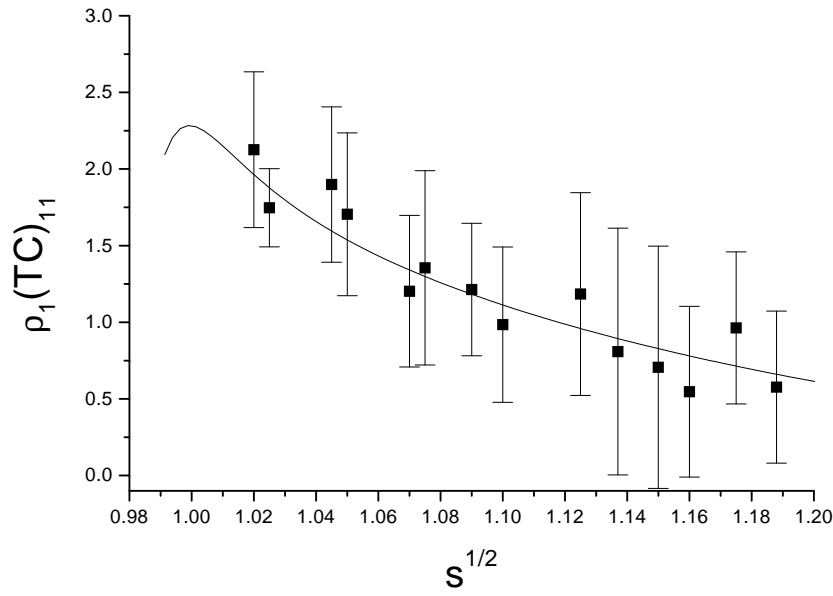FIG. 2. A typical fit to $\sin(2\delta_\pi)$ in the single channel unitarity region.

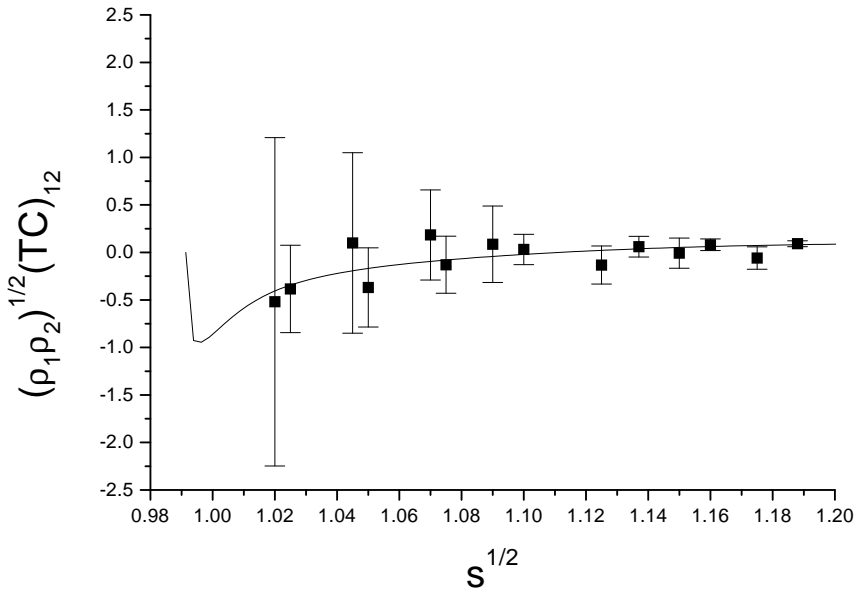FIG. 3.   A typical fit to $\mathbf{TC}_{11}$ in the coupled–channel unitarity region.

FIG. 4.   A typical fit to $\mathbf{TC}_{12}$ in the coupled–channel unitarity region.
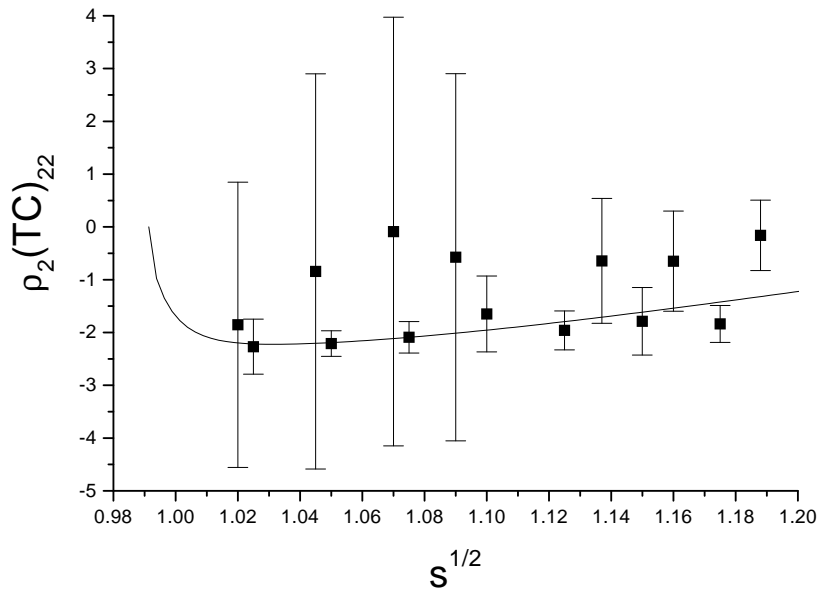
FIG. 5. A typical fit to $\mathbf{TC}_{22}$ in the coupled–channel unitarity region.